Wasit Journal of Engineering Sciences

Journal homepage: https://ejuow.uowasit.edu.iq

The influence of the working fluid and regenerator material on the performance of the types Gamma Stirling engine

Yahya Abbas Gbashi* and Ali A. F. Al-Hamadani

Affiliations
Department of Mechanical Engineering, Wasit University, Wasit, Iraq

Correspondence
Yahya Abbas Gbashi
Department of mechanical Engineering, Wasit University
Waist, Iraq
Email:
yahya a301@uowasit.edu.iq
aalhamadan i@uowasit.edu.iq

Received
10-August-2022
Revised
03-October-2022
Accepted
02-November -2022

Doi: 10.31185/ejuow.Vol10.Iss3.336

Abstract

In concentrated solar energy applications, the Stirling engine is the optimum option for extracting mechanical work. The engine's most notable features are minimal noise, vibration, and pollution, as well as its capacity to function with any external heat source, including biomass, solar energy, and industrial waste. The gamma-type STE-1008 Stirling engine is the subject of our research. This engine can handle a maximum charging pressure of 10 bar. The engine is divided into two sections (expansion and compression) and three heat exchangers (regenerator, cooler, and heater). The cooler is a finned aluminium heat exchanger with 144 internal fins, each with a cross-sectional area of 1 mm by 10 mm. The regenerator is fitted with a diameter of 31 m and a volumetric porosity of 90%. This investigation employed a random fiber with three different metals: stainless steel, copper, and aluminium. Nitrogen and air served as the working fluids. From the results, stainless steel, copper, and aluminium regenerators produced 583 W, 562 W, and 553 W, respectively. When nitrogen is utilized at 500 °C, the engine generates 11 N.m of torque compared to 8.5 N.m when air is used, and the engine has a thermal efficiency of 19% compared to 15% when air is used. The results of other researchers were used to compare and validate our model. With errors of no more than 12%, the results were close enough to the experimental data to be useful.

Keywords: Stirling engine, Regenerator material, Working fluid. STE1008, Nitrogen.

الخلاصة: في تطبيقات الطاقة الشمسية المركزة ، يعتبر محرك "ستيرلنغ" الخيار الأمثل لاستخراج الأعمال الميكانيكية. تتمثل أبرز ميزات المحرك في الحد الأدنى من الضوضاء والاهتزاز والتلوث ، فضلاً عن قدرته على العمل مع أي مصدر خارجي للحرارة ، بما في ذلك الكتلة الحيوية والطاقة الشمسية والنفايات الصناعية. إن محرك ستيرلينغ STE-1008 من نوع جاما هو موضوع بحثنا. يمكن لهذا المحرك التعامل مع أقصى ضغط شحن يبلغ 10 بار. ينقسم المحرك إلى قسمين (تمدد وضغط) وثلاثة مبادلات حرارية (مُجدد ، ومبرد ، وسخان). المبرد عبارة عن مبادل حراري من الألومنيوم بزعانف 144 زعنفة داخلية ، كل منها بمساحة مقطعية 1 مم × 10 مم. مُجدِّد مُجهز بقطر 31 ميكرومتر ومسامية حجمية 90٪. استخدم هذا التحقيق أليافًا عشوائية بثلاثة معادن مختلفة: الفولاذ المقاوم للصدأ والنحاس والألمنيوم. عمل النيتروجين والهواء كسوائل عمل. من نتائج مُجددات الفولاذ المقاوم للصدأ والنحاس والألمنيوم أنتجت 583 واط ، 562 واط ، 553 واط ، على التوالي. عند استخدام النيتروجين عند 500 درجة مئوية ، يولد المحرك 11 نيوتن متر من عزم الدوران مقارنة بـ 8.5 نيوتن متر عند استخدام الهواء ، وللمحرك كفاءة حرارية تبلغ 19٪ مقارنة بـ 15٪ عند استخدام الهواء. تم استخدام نتائج الباحثين الآخرين للمقارنة والتحقق من صحة نموذجنا. كانت النتائج قريبة بما يكفي لتكون ذات مغزى مقارنة بالبيانات التجريبية ، مع وجود أخطاء قصوى تبلغ 12٪.

1. INTRODUCTION

With the depletion of fossil fuels and the escalation of environmental concerns, the quest for a beneficial strategy to use renewable energy is critical now [1]. Stirling engines are attractive for this purpose because they emit less pollution, produce less noise, and are more efficient than other forms of heat engines [2]. Additionally, the Stirling engine demonstrates advantages in the exploitation of renewable energy, micro-cogeneration applications, and low-grade heat recovery [3]. Invention: Robert Stirling invented the Stirling engine in Scotland in the early nineteenth century [4]. Gheith et al. [5] studied experimentally the effect of regenerator materials on the performance of STE. They used four different materials: stainless steel, copper, aluminium, and Monel 400. Experimental studies have found that the stainless steel and Monel 400 regenerators provide 300 W and 253 W of braking power, respectively, at a pressure of 8 bar. Alfarawi et al. [6] constructed a thermodynamic model for Gamma-type STE simulation to determine the Influence of gas type and regenerator matrix type on the STE prototype. Helium and nitrogen were

employed as working gases. They found that shaft power increased by 49% in the case of helium and 35% in the case of nitrogen. Suyitno et al. [7] investigated the theoretical impacts of working fluids on the STE's performance. Air, an air-ethanol combination, and Also, nanofluids were employed. They discovered that nanofluid was more effective than an air-ethanol combination at increasing the STE's performance. The engine's maximum torque, power, and efficiency were 0.43 Nm, 16.67 W, and 5.95 percent, respectively. Katooli et al. [8] conducted a theoretical analysis of effective operational factors in the performance of gamma-type STEs. They examined operational parameters such as working fluid temperatures, engine speeds, and pressures. They worked with three different types of fluids: helium, nitrogen, and hydrogen. The findings indicated that the best fluid is hydrogen, followed by helium, which performs better than nitrogen, and lastly nitrogen, with the optimal engine speed being 1300 rpm. Sa'ed and Tlili [9] provide a numerical model for calculating and evaluating the ideal working fluid. They conducted tests on the engine using three different operating fluids: hydrogen, helium, and air. The results show that the engine power can be increased when the working fluid is changed and that the regenerator is to blame for the unwanted pressure drop as well as all of the excessive thermal losses. Chen et al. [10] experimentally studied parameters affecting engine performance, including the regenerator matrix material, the matrix wire diameter, and the fill factor. The findings revealed that stainless steel was the matrix material. results in a small increase in heat capacity, and copper results in a significantly increased heat transfer rate. They concluded that the 80-scale screen performs the best, while the 180-scale screen performs the worst. Oberweis and Al-Shemmeri [11] conducted a theoretical study of the effects of varying the charge pressure and working gas on the performance of the STE. The engine runs with three working fluids: air, hydrogen, and helium. The results show that using a lower density working gas would result in less loss than using a higher density working gas. Through previous studies, we did not find research on the STE-1008 gamma, and there is no modelling to know its thermal performance. In this paper, a theoretical study was conducted with the use of package software for the STE-1008. To know the effect of the filler metal on the regenerator The metals used were stainless steel, copper, and aluminium, with the use of air and nitrogen working fluids. To know the effect of the above factors on engine performance. The aim of the research is to study the performance of a Stirling engine STE-1008 with regeneration using the COMSOL program for three metals (stainless steel, copper, and aluminium) under the influence of changing the charging pressure and heating temperature using two types of gas (nitrogen and air).

2. ENGINE DESCRIPTION

Our study used the STE-1008 gamma-type Stirling engine (Figure 1). This engine has two work areas and three heat exchangers: a regenerator, a heater, and a cooler. The operating circumstances and geometrical characteristics of the Stirling engine are shown in Table 1. The regenerator is a heat exchanger made of stainless steel and composed of random fibres with a diameter of about 31 m and volumetric porosity of 90%, as shown in Figure 2. The heater shown in Figure 3, is a tubular type and consists of 20 tubes with an 8mm inner diameter made of stainless steel heated to 650°C via an electrical resistance (hot source). The cooler heat exchanger shown in figure (3.2) is a finned type made of aluminium and consists of 144 fins (10.5 mm×1mm) and is surrounded by a cooling water jacket, which takes the heat rejected from the working gas. Table 2 summarizes the various regenerator materials employed and their relative properties.

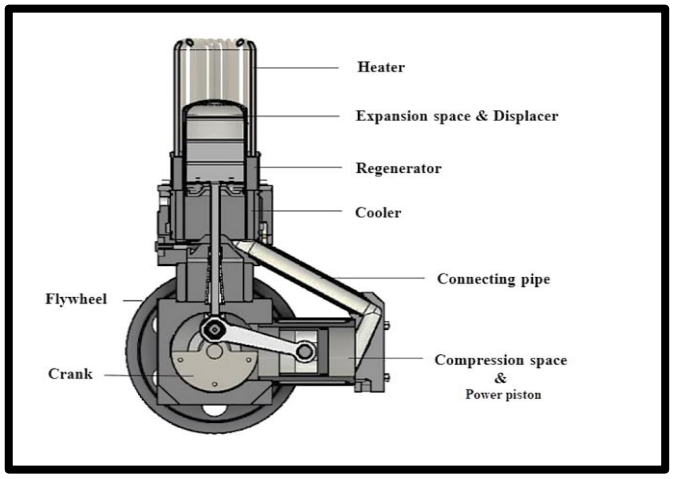

Figure 1: STE-1008 Gamma Stirling engine components [12].

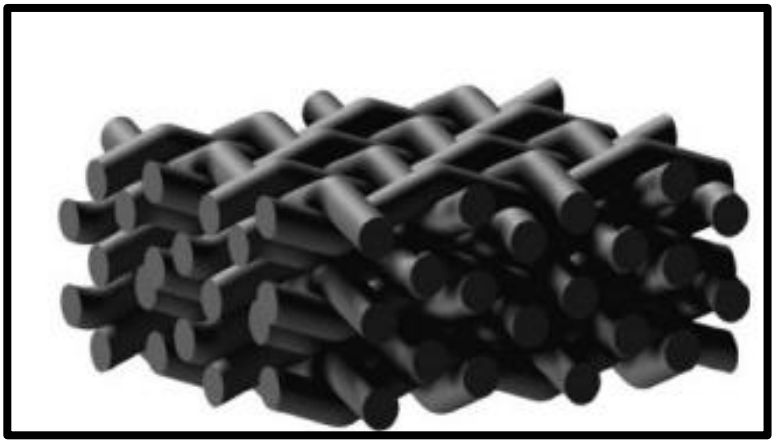

Figure 2: Regenerator Matrix [13].

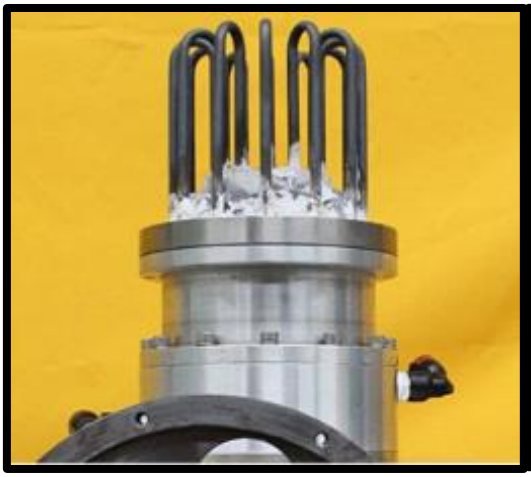

Figure3: The heater tubular [14**]**

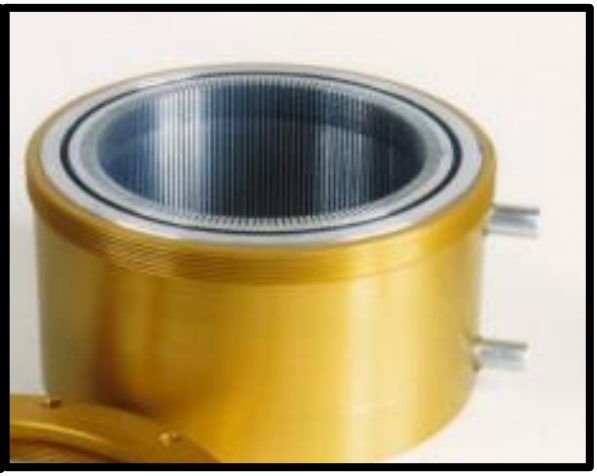

Figure 4: The cooler [15]

Table 1. STE-1008 Gamma Stirling Specifications of the engine. [19]

Variable	Value/description
Nominal rotational speed (rpm)	500
Stroke (mm)	75
Power piston bore (mm)	85
Charge pressure (bar)	10
Working gas	N2
Heater type	Tubular
Cooler type	Finned
Regenerator type	Random fiber
Wire diameter (μ m)	31
Porosity	0.9
Hot source temperature (°C)	650
Inlet water temperature (°C)	15
Water flow rate (L/min)	3.5
Water cooling power (kW)	2.3

Compression ratio	1.3

Table 2. Properties of all used regenerator materials [5].

Materials with porosity of 90%Stainless			
Proprieties	Stainless steel 4340	**Copper**	**Aluminium**
Density (kg.m^{-3})	7850	8920	2700
Thermal capacity (J.$kg^{-1}.k^{-1}$)	475	385	900
Thermal conductivity (W.$m^{-1}.\ k^{-1}$)	44.5	400	238

3. MATHEMATICAL MODEL

The Stirling engine's fundamental mechanics are inherently unstable. The heat transfer process occurs when a flow is oscillatory, laminar, or turbulent and compressible since the Stirling engine operates on the principle of gas expansion and compression. This complex physics with geometrical implications can all be managed by software [16]. The gas phases in porous media and governing equation environments include continuity, momentum, and energy equations [17].

$$\frac{\partial \rho}{\partial t} = \frac{\nabla . (\rho u)}{\varepsilon} \tag{1}$$

$$\frac{\rho}{\varepsilon}\left[\frac{\partial u}{\partial t} + (\mathrm{u}.\nabla)\frac{u}{\varepsilon}\right] = -\nabla \mathrm{P} - \frac{\nabla .\tau}{\varepsilon} - \left(\frac{\mu}{K} + \beta_f . |u|\right)u \tag{2}$$

$$\rho C_p \left[\varepsilon \frac{\partial T}{\partial t} + (\mathrm{u}\ .\ \nabla\ )\mathrm{T}\ \right] = \nabla .\ (\ \mathrm{k}\nabla \mathrm{T}\ ) + \frac{\tau .\nabla\ u}{\varepsilon} + \varepsilon\ \frac{D_P}{D_t}\ - \mathrm{Nu}\ \frac{K}{d_h}\ a_{Sf}\ (\ \mathrm{T} - T_s\ ) \tag{3}$$

Using real-time piston motion equations, the displacer and power pistons are defined in advance. [18].

$$X_e = \mathrm{r}\ [\ 1 - \ cos\ cos\ \theta\ + \frac{1}{\lambda_e}\ (\ 1 - \sqrt{1 - \lambda_e^2\ sin^2\theta}\ \ )] \tag{4}$$

$$X_{c\,=}\ \mathrm{r}\ [\ 1 - \ (\ \cos\ (\ \theta\ - \frac{\pi}{2}\ ) + \frac{1}{\lambda_e}\ (\ 1 - \sqrt{1 - \lambda_c^2 sin^2}(\theta - \frac{\pi}{2}))] \tag{5}$$

3.1. Moving part (piston ،displacer)

- Moving with velocity (dynamic mesh)
- Continuous thermal boundary condition

$$\mathrm{T_f} = \mathrm{T_S} \tag{6}$$

$$-\mathrm{K_f}\frac{\partial \mathrm{T_f}}{\partial \mathrm{n}} = -\mathrm{K_s}\frac{\partial \mathrm{T_s}}{\partial \mathrm{n}} \tag{7}$$

Stationary part (regenerator, cooler, heater):

1- Cooler

$$\mathrm{T} = \mathrm{T_c} \tag{8}$$

u = v = w = 0, no slip

2- Regenerator

$$\mathrm{u} = \mathrm{v} = \mathrm{w} = 0, \text{ no slip} \tag{9}$$

3- Heater

$$\mathrm{T} = \mathrm{T_h} \tag{10}$$

u = v = w = 0, no slip

In Computational Fluid Dynamics (CFD) modelling, the mesh quality affects the speed and accuracy of the result. As a result, the meshing size, time-stepping, and tolerances for the CFD model were carefully configured. Figure 3 shows the computational domain of the engine design. The heater tubes, displacer cylinder, regenerator, cooler, as well as the displacer as a solid substance, all nearly replicate the engine's actual form. The geometry also includes the appendix space between the displacer and the cylinder (see Fig 3). All simulations are done on a PC equipped with an Intel (R) Core (TM) i9-4820K processor running at 3.9 GHz and 64 GB of RAM. This research used an extremely thin triangular mesh, as shown in Figure 4. There are 39,806 elements in all, with an average element quality of 0.8. The influence of five different meshing sizes on CFD results is shown in table 3. Indicated power is the most important variable to decide the best mesh size. Therefore, a 0.0017% deferral ratio is very suitable between the two last values.

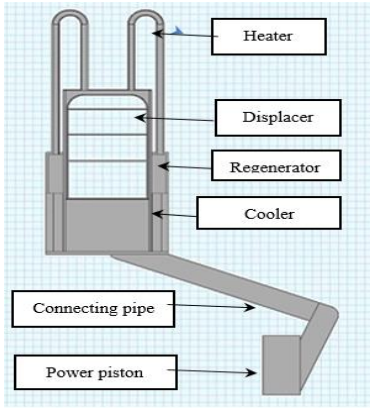

Figure 5: The engine's 2D computational domain.

Table 3. The sequence of meshes and CFD results.

Mesh sequence	No of elements	Indicated power
Extremely coarse	16018	566.79 W
Extra coarse	27179	579.14 W
Coarser	34569	582.51 W
Extremely fine	39806	583.64 W
Extremely fine	42428	583.63 W

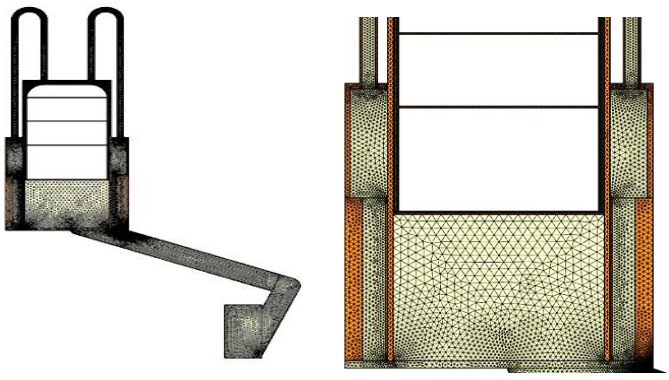

Figure 6: Meshing of engine domains.

The displacer and power piston walls have to move and have sliding walls affixed to them. Displacer and power pistons' movement bounds are specified by the equations that describe the pistons' true motion. The displacers outside walls are all moving except for the y-direction vertical wall, which is a sliding wall. The free movement of the displacer itself facilitates the free movement of the displacer's displacer cylinder's inner vertical walls. A boundary in physical contact with the piston in the x-direction also two additional walls (parallel to the x-orientation) that follow the piston's prescribed motion are considered moving walls for the x-direction boundary. For the sake of speeding up the computation, it is only enabled in the compression and expansion spaces and not in other domains (regenerator, heater, cooler, and pipe). The remaining walls are handled as adiabatic, save for the heater and cooler's constant temperature walls. Heat transfer with no flow conditions was used as a starting condition for the solution of the governing equations in a time-dependent fashion (no piston motion). Due to the engine's well-known temperature gradient, a steady-state solution may greatly reduce the amount of time it takes to do calculations.

4. COMSOL SOFTWARE SIMULATION

COMSOL multiphasic is a multiphasic simulation program and a cross-platform finite element analysis solver. Both conventional physics-based user interfaces and linked partial differential equation systems (PDEs) are supported. Each simulation can link to or communicate with other simulations using the COMSOL Multiply program [21]. Engineers and scientists use the COMSO Multiphysics software to simulate designs, devices, and processes in all fields of engineering, manufacturing, and scientific research. Computer simulation has become an essential part of science and engineering. Digital analysis of components, in particular, is important when developing new products or optimizing designs. Today, a broad spectrum of options for simulation is available; researchers use everything from basic programming languages to various high-level packages implementing advanced methods. COMSOL [22] is a flexible platform that allows users to model all relevant physical aspects of their designs.

5. RESULTS AND DISCUSSION

4.1 Validation with other study

When the current study was compared to a similar one [5], Although there is a discrepancy between the two studies, the indicated power of the current research is higher than that of the previous match study for regeneration metal fabrication. With a heating temperature of 500 °C and a charging pressure of 8 bar, the study found that the power was 299 W. While the power indicated for the previous research was 280 W for the same conditions as shown in Figure 7, the maximum error was 12%. Figure 8. The stated power predicted for various charge pressures is very close to the observed values. The pattern is comparable to an experiment. However, power is over-predicted with a maximum error of 12%. This may be attributed to the uncertainty in heat losses in the experiment part and affects the computation of indicated power. Table 4 shows the details of the validation parameters with which it was compared.

Table 4. Details of the parameters used in the valuation

Parameters	Values
Maximal rotation speed	600 rpm
Working fluid	air
Temperature of the cold source	15°C
Porosity	90%
Temperature of the hot source	15°C
Porous media	Stainless steel
Temperature of the hot source	500°C
Power piston bore	80 mm
Stroke	145 mm
Outside diameter regenerator	134 mm
Inside diameter regenerator	98 mm
Height	50 mm

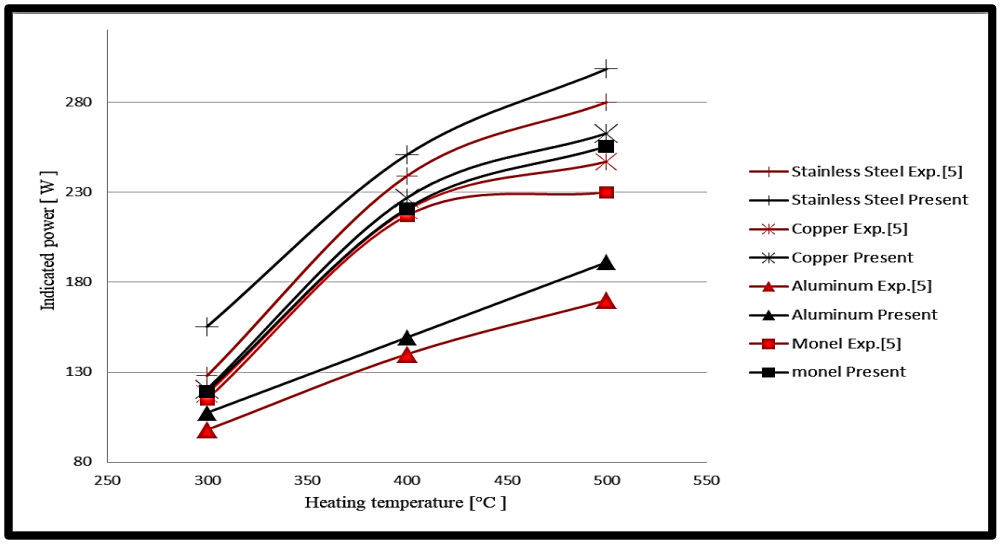

Figure 7: Comparison of current and experimental air results at a fixed charge pressure (8 bar) and various heater temps

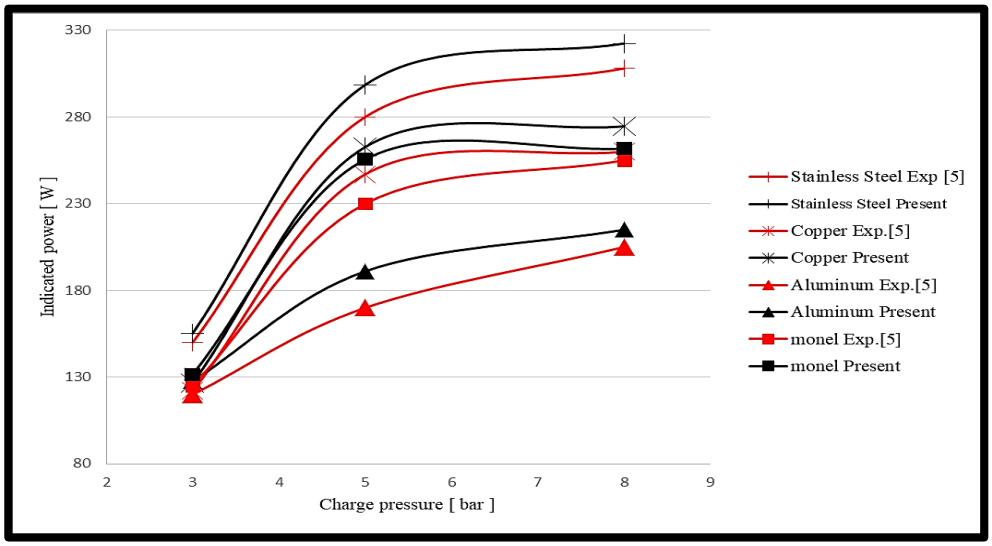

Figure 8: Comparison of current and experimental air outcomes at a given heater temperature (500 °C) and various charge pressures.

4.2. Normal operating conditions

The simulated engine's general results are reported in this section. The engine's operational conditions were originally mentioned in Table1. In Figure 9 (a), through the connecting pipe, the compressed gas exits the compression area. Due to the unbalanced geometry, it separates into two streams. A portion of the gas mass passes through the coolers. Meanwhile, the second part enters the expansion space below the displacement piston. The majority of the gas is contained in the engine's lower section and also cooled via a cooling water jacket. The displacer travels down, and the power piston makes a right-hand turn. Compression commences at the start of each new cycle and continues until the power piston hits the top dead centre (TDC). Due to increased loss of inertia in matrix pore volumes, during the cycle, the regenerator experiences the largest pressure decrease. The gas phase's outline temperature over the engine spaces is seen in Figure 9 (c), where the gas from the heater passes through the regenerator. Energy is released into the matrix and then departs at a temperature that is often greater than the final temperature of the cold season. This is dependent on the thermal losses and the regenerator's efficacy.

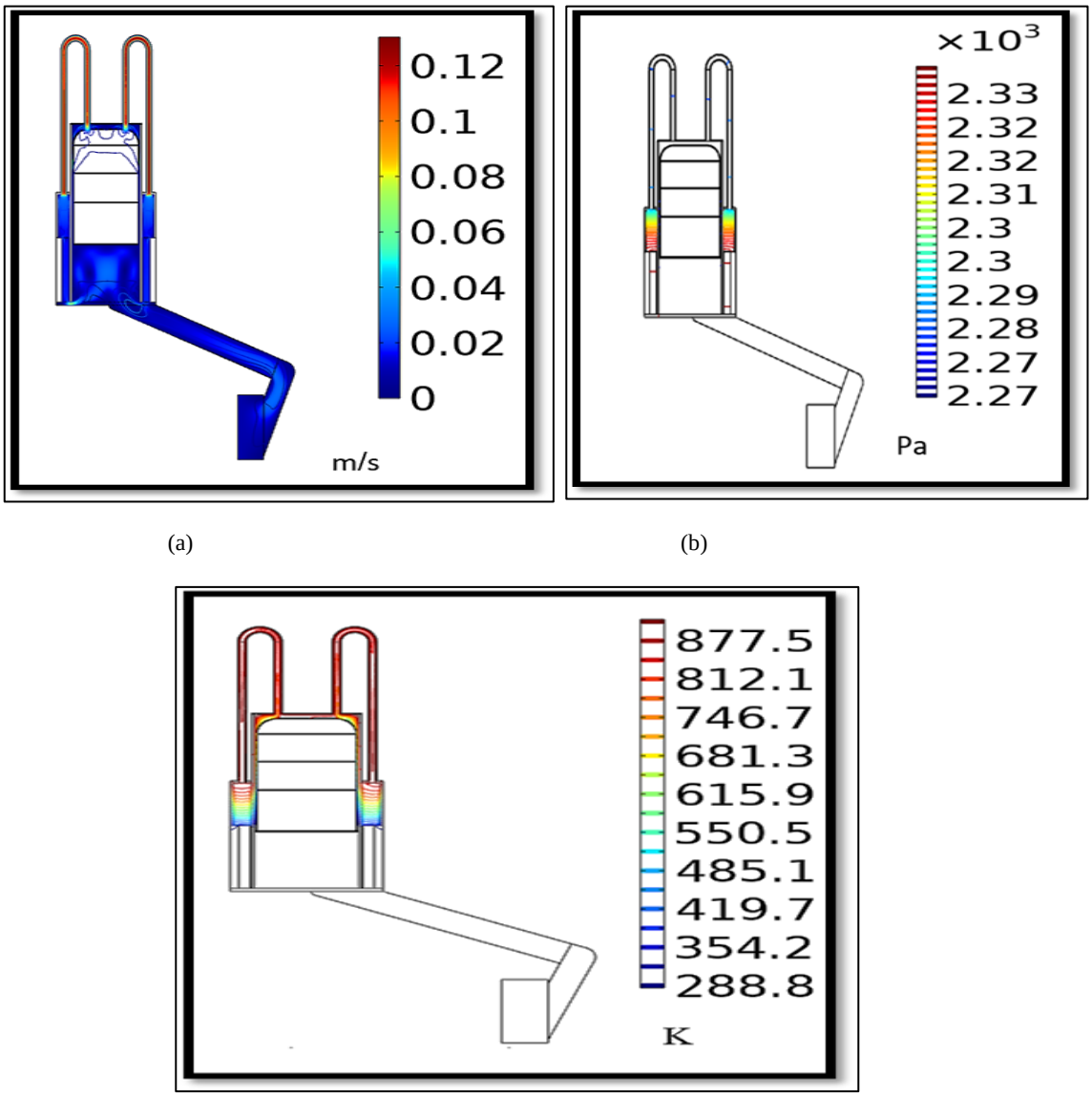

(a) (b)

Figure 9: Normal operating conditions of the engine: (a) velocity contour, (b) pressure contour, and (c) temperature contour.

4.3. Effect of regeneration materials on engine performance

Figure 10. For all temperatures, the Stirling engine showed power for the various regenerator materials. The temperature gradient between the two regenerator sides is lowest on the aluminium regenerator. In a Stirling engine, raising the starting charge pressure concurrently increases the mass, density, and velocity of the working fluid, hence increasing the amount of work done by the engine. The increase in heating temperature decreases both the working fluid temperature and the temperature gradient between the two heat sources. The next section details the heating temperatures of 300 °C, 400 °C, and 500 °C, as well as the starting charge pressures of 3 bar, 5 bar, and 8 bar. Figure 10 illustrates the relationship between stated power and charge pressure and regenerator materials. The stated power grows with the starting charge pressure for all regenerator materials investigated. The regenerator made of stainless steel provided the highest stated power (about 583. W for Pi = 5 bar). The aluminium regenerator generates the minimum indicated power (about 553 W for Pi = 5 bar).

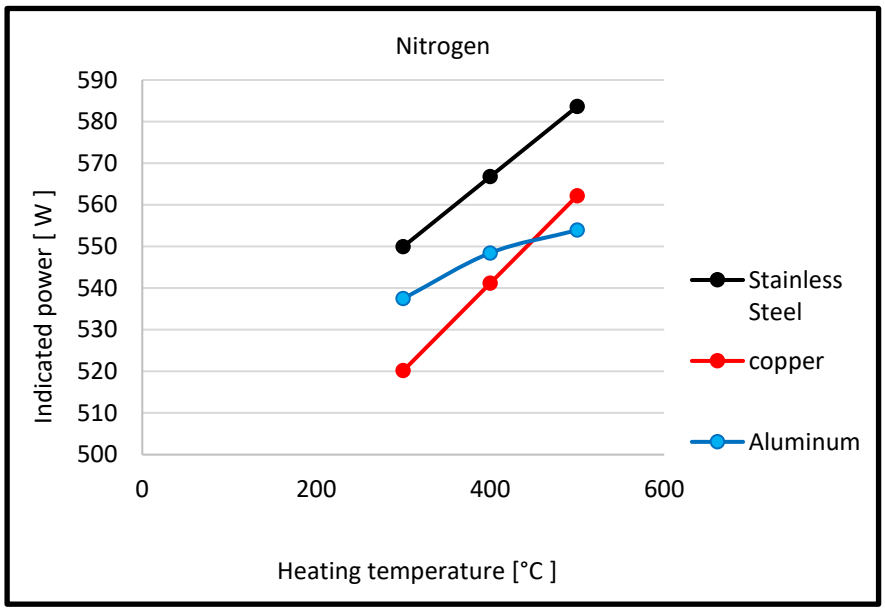

Figure 10: The Stirling engine showed the indicated power of the various regenerator materials at all temps studied at a speed of 500 rpm.

In Figure 11, the copper regenerator produced equivalent indicated power to that of the stainless-steel regenerator. However, its stated power output is smaller than that of the stainless-steel regenerator at high heating temperatures. The high thermal conductivity of copper means that as the heating temperature goes up, more heat is lost through the shuttle effect and internal conduction.

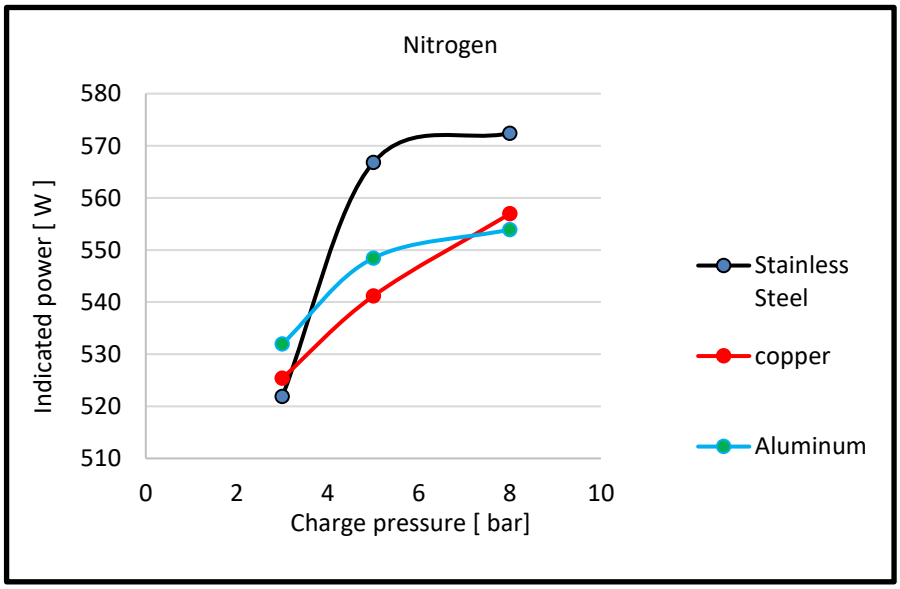

Figure 11. For all investigations, the Stirling engine showed power for the various regenerator materials at charge pressures of nitrogen gas and a speed of 500 rpm

Figure 12 presents the changes in the indicated power produced by regenerator materials with the change in the hot source temperatures with the use of air as a working fluid. As the heat source increases, the power supply also increases. The maximum indicated power with stainless steel and the minimum indicated power with copper were

452 W and 392 W, respectively, at a hot source temperature of 500 °C. This is due to the heat capacity of stainless steel being larger than the other materials.

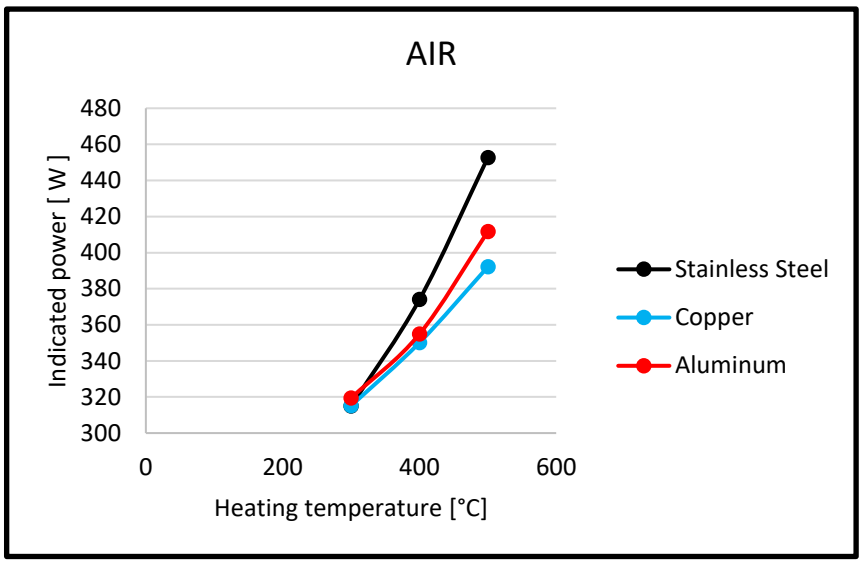

Figure 12: The Stirling engine showed the indicated power of the various regenerator materials and air at all temperature studied at a speed of 500 rpm.

Figure 13 demonstrates the variance in stated power with charge pressures when air is used as the working fluid and for all three regenerated engine metals: stainless steel, copper, and aluminium. The increase in the charging pressure for all aluminium states increases the engine power. At a charge pressure of 8 bar, the indicated power of the stainless steel was 492 W and the aluminium and copper were 386 W and 361 W, respectively.

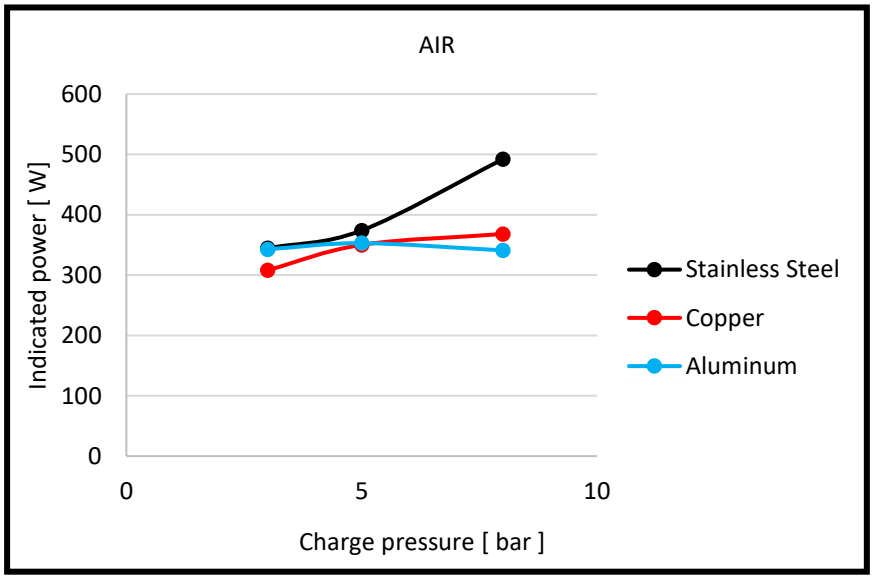

Figure 13: For all investigations, the Stirling engine showed power for the various regenerator materials at charge pressures of air gas and a speed of 500 rpm.

4.4. Effect of gas type on engine torque and thermal efficiency

Figure 14 demonstrates the influence of gas type on engine performance at varying temperatures from the hot source. When it is noticed that nitrogen is utilized, when the engine's hot source temperature is increased, the engine's torque

values are superior to those of air. Up to hot source temperature to 300 °C. At 500 °C, the engine produces a torque of 11 N.m when using nitrogen compared to 8.6 N.m when using air. Nitrogen has a higher heat capacity than air.

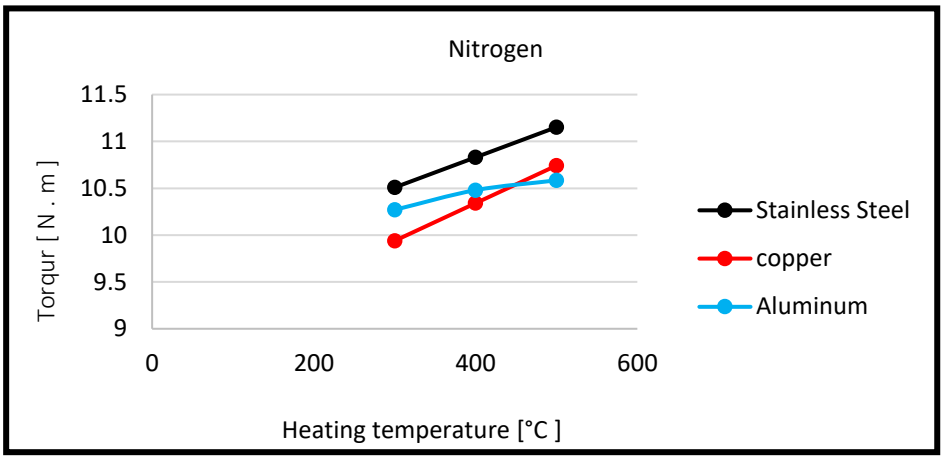

(a) Nitrogen

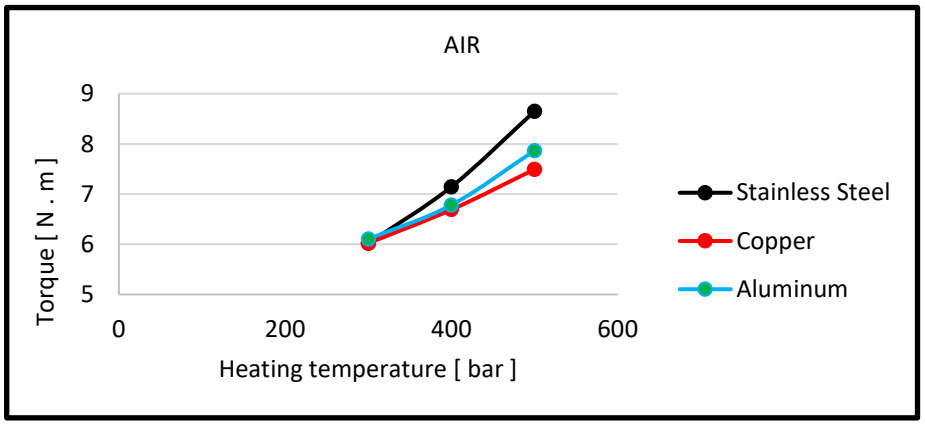

(b) Air.

Figure 14: Effect of gas type on engine torque, (a) Nitrogen, and (b) Air.

Figure 15 shows that at various charge pressures, the influence of gas type on engine performance is examined. On the thermal efficiency of nitrogen and air as working gases (in the range of 3bar to 8bar). Thermostatic efficiency increases with charge pressure for nitrogen and air. An 8-bar engine produces a thermal efficiency of 19% when using nitrogen compared to 16.8% when using air. The thermal conductivity of nitrogen is greater than that of air.

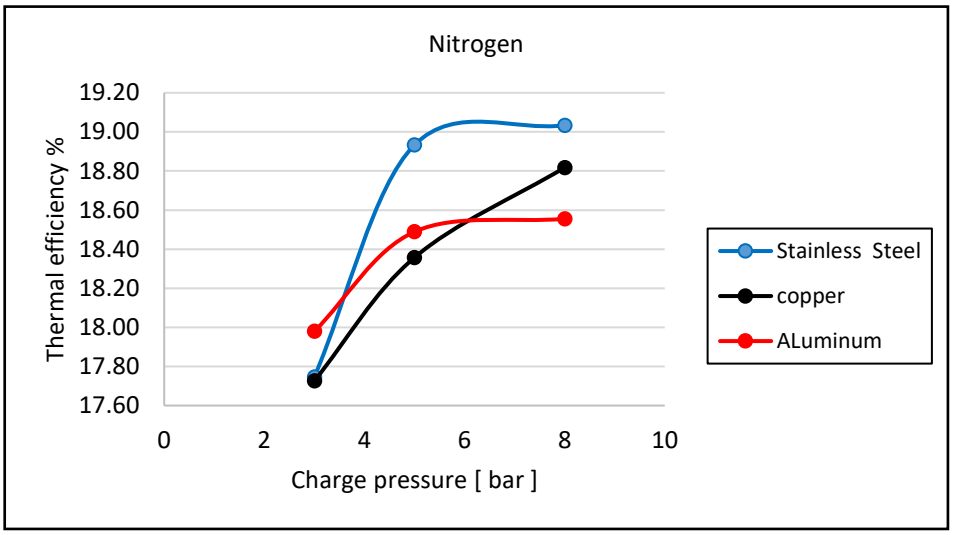

(a) Nitrogen

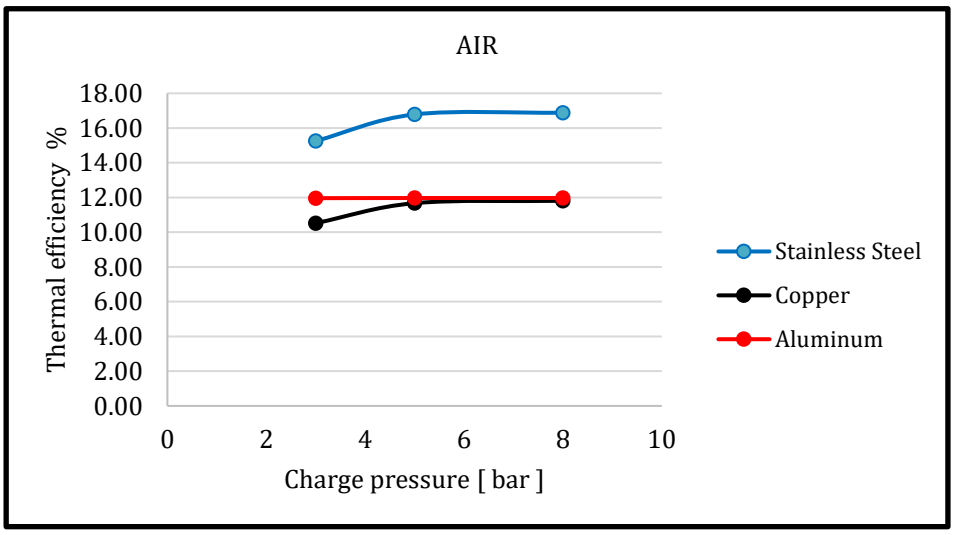

(b)Air

Figure 15: Effect of gas type on thermal engine, (a) Nitrogen and (b) Air

5. CONCLUSION

- Three regenerator matrices were investigated, each with a different constituent material: stainless steel, copper, and aluminium. The regenerators made of stainless steel have an adequate thermal efficiency.
- The regenerators of stainless steel, copper, and aluminium produce 583W, 562W, and 553W of indicated power for Pi = 5bar, respectively.
- Having a heat capacity and a thermal exchange rate, stainless steel regenerators are found to be the best Stirling engine regenerators when compared to the other materials investigated.
- Increased charge pressure and heating temperature result in a rise in the indicated power and efficiency of the Stirling engine.
- A max error of 12% has been discovered between the model and experimental data.
- The effect of gas type on engine performance was investigated using two working fluids: nitrogen and air. It is noted that when nitrogen is used, the engine produces a torque of 11 N.m compared to 8.6 N.m when using air.
- The performance of engines is improved because nitrogen has a higher heat capacity than air and produces more power.

Nomenclature

c_p	gas heat capacity, J/kg.K
d_h	hydraulic diameter, m
K	permeability, m^2
k	gas thermal conductivity, W/m.K
Nu	Nusselt number
P	instantaneous gas pressure, Pa
T	gas-phase temperature, ℃
T_S	solid-phase temperature, ℃
r	Crank radius, mm
u	velocity magnitude in x direction , m/s
Xc	power piston displacement, m
Xe	displacer piston displacement, m
STE	Stirling Engine
k_f	Fluid Thermal conductivity,W/m. K
k_s	solid thermal conductivity, W/m.K
T_h	Temperature Heater, K
T_c	Cooler temperature ,K
T_f	Fluid Temperature,K
v	velocity magnitude in y direction , m/s
w	velocity magnitude in z direction , m/s

Greek letters

β_f	Forchheimer drag coefficient, kg/m^4
λ_c	Crank radius to compression connecting rod ratio.
λ_e	Crank radius to expansion connecting rod ratio.
θ	Crank angle, rad
ρ	gas density, kg/m^3
μ	gas dynamic viscosity, Pa.s
ε	porosity

References

1. M. J. Li, Y. L. He, and W. Q. Tao, "Modeling a hybrid methodology for evaluating and forecasting regional energy efficiency in China," *Appl. Energy*, vol. 185, no. 2017, pp. 1769–1777, 2017, DOI: 10.1016/j.apenergy.2015.11.082.
2. M. H. Ahmadi, M. A. Ahmadi, and F. Pourfayaz, "Thermal models for the analysis of the performance of Stirling engine: A review," *Renew. Sustain. Energy Rev.*, vol. 68, no. July 2015, pp. 168–184, 2017, DOI: 10.1016/j.rser.2016.09.033.
3. K. Wang, S. R. Sanders, S. Dubey, F. H. Choo, and F. Duan, "Stirling cycle engines for recovering low and moderate temperature heat: A review," *Renew. Sustain. Energy Rev.*, vol. 62, no. September 2018, pp. 89–108, 2016, DOI: 10.1016/j.rser.2016.04.031.
4. D. G. Thombare and S. K. Verma, "Technological development in the Stirling cycle engines," *Renew. Sustain. Energy Rev.*, vol. 12, no. 1, pp. 1–38, 2008, DOI: 10.1016/j.rser.2006.07.001.
5. R. Gheith, F. Aloui, and S. Ben Nasrallah, "Study of the regenerator constituting material influence on a gamma type Stirling engine," *J. Mech. Sci. Technol.*, vol. 26, no. 4, pp. 1251–1255, 2012, DOI: 10.1007/s12206-012-0218-9.
6. S. Alfarawi, R. Al-Dadah, and S. Mahmoud, "Enhanced thermodynamic modeling of a gamma-type Stirling engine," *Appl. Therm. Eng.*, vol. 106, pp. 1380–1390, 2016, doi: 10.1016/j.applthermaleng.2016.06.145.
7. W. E. Juwana, O. Dwi, H. Putra, and S. Huda, "Effects of Working Fluids on the Performance of Stirling Engine The 12th Annual National Seminar Of Mechanical Engineering (SNTTM XII) Effects of Working Fluids on the Performance of Stirling

Engine," no. October 2013, DOI: 10.13140/2.1.2365.3125.
8. M. H. Katooli, R. Askari Moghadam, and M. Hooshang, "Investigation on effective operating variables in gamma-type Stirling engine performance: a simulation approach," *SN Appl. Sci.*, vol. 2, no. 4, pp. 1–7, 2020, DOI: 10.1007/s42452-020-2526-5.
9. M. Khmelniuk, V. Trandafilov, O. Ostapenko, and Y. Baidak, "Numerical investigation of working fluid influence on Stirling refrigeration machine performance," *Refrig. Sci. Technol.*, vol. 2017-Septe, no. 1, pp. 6–9, 2017, doi: 10.18462/iir.compr.2017.0211.
10. W. L. Chen, K. L. Wong, and H. E. Chen, "An experimental study on the performance of the moving regenerator for a γ-type twin power piston Stirling engine," *Energy Convers. Manag.*, vol. 77, pp. 118–128, 2014, DOI: 10.1016/j.enconman.2013.09.030.
11. S. Oberweis and T. T. Al-Shemmeri, "γ-Stirling engine – The effect of different working gases and pressures," *Renew. Energy Power Qual. J.*, vol. 1, no. 9, pp. 315–320, 2011, doi: 10.24084/repqj09.322.
12. "Stirling School of Engines." [Online]. Available: http://stirlingmotor.ir/. [Accessed: 25-Aug-021].
13. M. B. Ibrahim and R. C. Tew Jr, Stirling convertor regenerators: CRC Press, 2011.
14. C.-H. Cheng, H.-S. Yang, and L. Keong, "Theoretical and experimental study of a 300-W beta-type Stirling engine," *Energy*, vol. 59, pp. 590-599, 2013
15. A.Ross, Making stirling engines: Ross experimental, 1993.
16. B. Kongtragool and S. Wongwises, "A review of solar-powered Stirling engines and low-temperature differential Stirling engines," *Renew. Sustain. Energy Rev.*, vol. 7, no. 2, pp. 131–154, 2003, DOI: 10.1016/S1364-0321(02)00053-9.
17. R. Tew, T. Simon, D. Gedeon, M. Ibrahim, and W. Rong, "An initial non-equilibrium porous-media model for CFD simulation of Stirling regenerators," Collect. Tech. Pap. - *4th Int. Energy Convers. Eng. Conf.*, vol. 1, pp. 65–77, 2006, DOI: 10.2514/6.2006-4003.
18. A. Wagner, "Calculations and experiments on Gamma-type Stirling engines," no. March, p. 307, 2008, [Online]. Available: http://orca.cf.ac.uk/54 057/1/U585566pdf.
19. S. Alfarawi, R. AL-Dadah, and S. Mahmoud, "Influence of phase angle and dead volume on gamma-type Stirling engine power using CFD simulation," *Energy Convers. Manag.*, vol. 124, no. February 2020, pp. 130–140, 2016, doi: 10.1016/j.enconman.2016.07.016.
20. J. K. Ferrell and E. P. Stahel, "Heat transfer," *Ind. Eng. Chem.*, vol. 58, no. 12, pp. 42–54, 1966, doi: 10.1021/ie50684a008.
21. C. Multiphysics, "COMSOL Multiphysics Programming Reference Manual 5.6," 2020.
22. V. Bhaskar, "Introduction to COMSOL Multiphysics Introduction to C omsol Multiphysics,. COMSOL Multiphysics, Burlington, MA, 1998.